Clinical applicability of *in vivo* fluorescence confocal microscopy for noninvasive diagnosis and therapeutic monitoring of nonmelanoma skin cancer

Susanne Astner
Charité-Universitätsmedizin Berlin
University Medical School
Department of Dermatology, Venerology and Allergology
and
Skin Cancer Center
100117 Berlin, Germany

Susanne Dietterle
Nina Otberg
Charité-Universitätsmedizin Berlin
University Medical School
Department of Dermatology, Venerology and Allergology
and
Center of Experimental and Applied Skin Physiology
100117 Berlin, Germany

Hans-Joachim Röwert-Huber
Eggert Stockfleth
Charité-Universitätsmedizin Berlin
University Medical School
Department of Dermatology, Venerology and Allergology
and
Skin Cancer Center
100117 Berlin, Germany

Jürgen Lademann
Charité-Universitätsmedizin Berlin
University Medical School
Department of Dermatology, Venerology and Allergology
and
Center of Experimental and Applied Skin Physiology
100117 Berlin, Germany

Abstract. Excisional biopsies and routine histology remains the gold standard for the histomorphologic evaluation of normal and diseased skin. However, there is increasing interest in the development of noninvasive optical technologies for evaluation, diagnosis, and monitoring of skin disease *in vivo*. Fluorescent confocal microscopy is an innovative optical technology that has previously been used for morphologic evaluation of live human tissue. We evaluate the clinical applicability of a fluorescent confocal laser scanning microscope (FLSM) for a systematic evaluation of normal and diseased skin *in vivo* and in correlation with routine histology. A total of 40 patients were recruited to participate in the study. Skin sites of 10 participants with no prior history of skin disease served as controls and to evaluate topographic variations of normal skin *in vivo*. Thirty patients with a suspected diagnosis of nonmelanoma skin cancer were evaluated, whereby FLSM features of actinic keratoses (AK) and basal cell carcinoma (BCC) were recorded in an observational analysis. Selected BCCs were monitored for their skin response to topical therapy using Imiquimod as an immune-response modifier. A commercially available fluorescence microscope (OptiScan Ltd., Melbourne, Australia) was used to carry out all FLSM evaluations. Common FLSM features to AK and BCC included nuclear pleomorphism at the level of the granular and spinous layer and increased vascularity in the superficial dermal compartment. Even though the presence of superficial disruption and mere atypia of epidermal keratinocytes was more indicative of AK, the nesting of atypical basal cells, increased blood vessel tortuosity, and nuclear polarization were more typical for BCC. All diagnoses were confirmed by histology. FLSM allowed a monitoring of the local immune response following therapy with Imiquimod and demonstrated a continuous normalization of diseased skin on repeated evaluations over time. This study illustrates potential applications of FLSM in clinical dermatology for the evaluation of dynamic skin conditions and monitoring of cutaneous response to noninvasive therapies. The findings are of preliminary nature and warrant further investigations in the future.
[DOI: 10.1117/1.2837411]

Keywords: *In vivo* confocal microscopy; nonmelanoma skin cancer; actinic keratoses; basal cell carcinoma.

Paper 07050RR received Feb. 14, 2007; revised manuscript received Aug. 29, 2007; accepted for publication Sep. 25, 2007; published online Feb. 19, 2008.

1 Introduction

Conventional histopathology remains the gold standard for microscopic evaluation of skin histopathology. Tissue excision, processing, sectioning, and staining are required to allow light-microscopic analysis; yet although cellular details are visualized at high resolution, biopsies are painful, expensive, time-consuming, and associated with scar formation. Furthermore, routine histology does not allow repeated evaluations of dynamic processes over time, because the tissue under investigation is removed for evaluation. Finally, given anatomic variations and cellular pleomorphism, sampling errors remain a significant challenge in a variety of skin diseases with advanced cutaneous involvement such as nonmelanoma skin cancer (NMSC)[1,2] or T-cell lymphoma.[3]

Address all correspondence to: Prof. Dr. Jürgen Lademann, Ph.D., Charité-Universitätsmedizin Berlin, Center of Experimental and Applied Skin Physiology, Department of Dermatology, Venerology and Allergology, Charitéplatz 1, 10117 Berlin, Germany. Tel: +49-30-450-518-100; Fax: +49-30-450-518-918; E-mail: juergen.lademann@charite.de

1083-3668/2008/13(1)/014003/12/$25.00 © 2008 SPIE

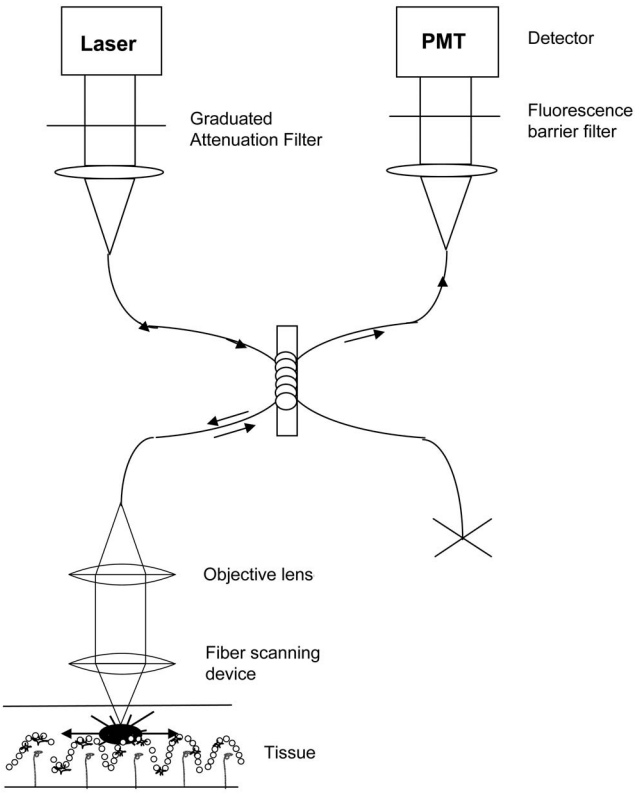

Fig. 1 Optical configuration scheme of FLSM. Modified from Suihoko et al. (Ref. 28).

Recent developments in optical imaging techniques may offer new avenues for real-time noninvasive, high-resolution analysis of skin and several of these technologies have become commercially available. Among these, optical coherence tomography (OCT), high-frequency ultrasound (HFUS), magnetic resonance imaging (MRI), multispectral fluorescence polarization imaging, TetraHertz imaging, near infrared and Raman spectroscopy, and reflectance or fluorescence confocal microscopy are the most promising for real-time evaluation of cutaneous tissue.[4–10] OCT, HFUS, and MRI obtain full thickness vertical optical sections that correlate well with the gross morphology of routine histology, yet the resolution is limited and does not reach cellular levels. On the other hand, *in vivo* reflectance and fluorescence confocal microscopy (CM) generate horizontal optical sections at a resolution that is comparable to routine histology, but at the present time, these technigues are limited by their penetration depth.[11–16]

The underlying principle of fluorescent confocal laser scanning microscopy (FLSM) systems is the excitation and detection of fluorophores by scanning a focal plane within the tissue using a coherent laser light source. A fiber-optic coupler system separates tissue illumination from fluorescence detection, thereby enabling a high resolution of FLSM images of about 0.5 to 1 μm (Fig. 1).[14,15] Contrast and image interpretation is based on the presence of endogenous or exogenous fluorophores. In that respect, two sources of fluorescent molecules can be differentiated: autofluorescence (endogenous fluorophores) or applied fluorescent contrast agents (exogenous fluorophores).[12–14] Autofluorescence from flavins, porphyrins, and collagen has an excitation maximum at the spectrum of UV light, which—due to the shallow penetration of UV radiation—only provides a poor contrast signal. For clinical purposes in FLSM imaging, the application of exogenous "fluorescent dyes" is required to provide sufficient contrast within the tissue.[11]

To visualize cellular structures, lasers of different wavelengths may be used, yet although the longer wavelengths penetrate deeper into the skin, they also yield lower resolution compared to shorter wavelengths. The fluorescence confocal microscope (FLSM) used in this study employs an argon-ion laser at a wavelength of 488 nm for tissue illumination, but detection occurs at longer wavelengths. After excitation, the emitted fluorescence then allows visualization of the morphological details of cellular microstructures.[13,14] Image contrast is achieved through distribution and accumulation of exogenously applied fluorophores in the intercellular and intracellular compartments of live skin.[13,14]

Other confocal microscopy systems are based on reflectance measurements of structures with different refractive indices.[17–19] Melanin, hemoglobin, and other cellular microstructures with high-refractive indices produce strong backscatter with visible (400 to 700 nm) and near infrared (700 to 1064 nm) wavelengths, and the visualization of epidermal structures is based on differences in different structural reflectivity. In the case of reflectance confocal microscopy (RCM), systems illumination and detection takes place at the same wavelength. In both systems, when correlating CM images to routine histology, the major differences as compared to conventional histology are that the images are oriented horizontally to skin surface (*en face*) and that they are analyzed in gray scale.[18,19]

This study evaluates the clinical applicability of FLSM in the evaluation of normal and diseased skin *in vivo*. The evaluations were used to (a) describe topographic variations of normal skin and (b) evaluate nonmelanoma skin cancer noninvasively, in reference to normal skin and in correlation with vertical hematoxylin and eosin (H&E) histopathology. Lastly, (c) FLSM was used for noninvasive monitoring of skin disease and therapeutic response to novel treatment modalities over time.

2 Materials and Methods

2.1 *Study Participants*

Forty individuals aged between 37 and 67 years were asked to participate in this study. All patients were recruited from the Department of Dermatology at the University Hospital of the Charité, Berlin. Written consent was obtained prior to investigation. All research was conducted according to the Declaration of Helsinki principle.

2.2 *Fluorescence Confocal Laser Scanning Microscope*

A commercially available FLSM (OptiScan Ltd., Melbourne, Australia) was used in this study. A comprehensive review of the optical principles has been published elsewhere.[12,13]

The system is equipped with a single-moded optical fiber incorporated into a handheld scanning device, which is used for both illumination of the tissue and detection of fluorescence signals. A coherent argon-ion laser light source at a

wavelength of 488 nm is used to illuminate the tissue, thereby exciting the fluorescent molecules within the specimen to a singlet state. Upon returning to their respective ground states, the wavelengths emitted by these fluorophores are longer than illumination wavelengths, permitting them to be propagated through the optical fiber. A fiber-optic coupler separates the shorter wavelengths used for illumination from the longer wavelengths returning from the focal point within the tissue, and signals are then propagated to the photomultiplier tube (PMT) for detection. Light coming from out-of-focus planes will not be propagated, thus enabling the high resolution of FLSM images. Similarly, reflected or backscattered laser light is eliminated by a fluorescence barrier filter, only permitting longer wavelengths corresponding to fluorescence signals to pass through to the filter. Tissue emitted fluorescence is then focused onto a PMT for detection, generating images of a lateral resolution of approximately 0.5 to 1 μm and an axial resolution (section thickness) of 3 to 5 μm. Images are resolved in 12-bit gray scale and the scanned field of view (FOV) is 250×250 μm producing images of 1024×1024 pixels. Based on a 250-μm FOV, when this is displayed on the standard 19-in monitor on the Stratum used in the present study, the displayed image is approximately 25×25 cm, which equates to approximately $1000\times$ magnification. The numerical aperture (NA) of the system was 0.5, illumination power on tissue level was less then 0.5 mW. Figure 1 illustrates the optical scheme of FLSM.

Briefly, after intraepidermal injection of 0.2% sodium fluorescein (0.02 to 0.05 ml total volume), the optical fiber is placed onto the skin using a handheld contact device without fixing the optical system to the patient's skin. By moving the objective lens in the z (vertical) direction with respect to the skin surface, it is possible to image at different horizontal planes within the tissue. During the imaging process, the depth level being imaged was ascertained by the morphological appearance of tissue or by using a micrometer attached to the z stage of the objective lens. By zeroing the imaging depth at the level of the most superficial layer before going vertically into the tissue, depth measurements can be obtained. By moving the tip of the scanning device in the x and y directions, different areas within the specimen are evaluated. To allow an evaluation of corresponding skin sites over time, skin markings were made using permanent marker on the day of the baseline evaluation, whereby skin sites were determined for all followup evaluations. Additionally, a schematic depiction of the lesion and its outline was obtained on transparencies, such that by localizing anatomic hallmarks, relatively precise colocalization was possible over extended periods of time. Furthermore, four to six representative FLSM images of each level are obtained to demonstrate the reproducibility of each parameter and correct for potential variations with the tissue under investigation.

2.3 *Application of the Fluorescent Dye*

A 0.2% solution of sodium fluorescein (Fluorescein SE Thilo, Producer Alcon, France) was used as fluorescent dye and contrast agent for labeling of skin structures. The solution was administered under standardized conditions using a 1-ml tuberculin syringe fitted with a 32-gauge needle[13,14] for superficial, intraepidermal injection. The injected volume did not exceed a total volume of 10 to 20 μl and a 3 to 5-mm diameter area was infiltrated with fluorescein sodium. In addition, one drop of sodium fluorescein was applied onto the site of FLSM evaluation for labeling of skin surface structures. Exact placement of the syringe within the epidermal compartment was ensured by using a 5 to 10 deg angle with respect to the surface. Once intraepidermally injected, fluorescein is readily distributed within the skin. There is minimal pain associated with the insertion of the needle. In concordance with previous publications,[13,14] the administration of fluorescein was performed at approximately 5 to 10 min prior to the evaluation. The fluorophore is first detectable in the extracellular space, contrasting the intercellular compartment resulting in a bright white-gray contrast. It then diffuses into the cytoplasm and nuclei of epidermal keratinocytes, to finally be redistributed into the cytoplasm. Following fluorescein injection, a drop of immersion oil was applied to the sites selected for imaging, matching the refraction index of the stratum corneum ($n = 1.55$) to reduce backscatter and reflectance from surface structures.

2.4 *FLSM Measurements*

2.4.1 *FLSM evaluation of normal skin*

Ten individuals with no prior history of skin disease were systematically evaluated using FLSM to define the morphologic features of normal skin in variable anatomic skin sites. Our FLSM evaluation parameters were based on observations previously made by Swindle et al.[13,14] Sun-protected skin sites were evaluated by obtaining sequential images at matching skin sites of the volar aspect of the right or left forearm. Additional evaluations were performed on sun-exposed skin sites, by examining dorsal aspects of the forearms. For FLSM evaluation of eccrine glands and the influence of dry skin (xerosis) on the structural integrity of the skin, both palms and lower legs of each volunteer were imaged, respectively.

2.4.2 *FLSM evaluation of neoplastic skin lesions*

A total of 30 patients with a clinically suspected diagnosis of NMSC were evaluated using FLSM to define the histomorphometric features of NMSC in correlation with and reference to routine histology. All lesions were systematically evaluated for the presence or absence of characteristic features of actinic keratoses (AK) or basal cell carcinoma (BCC), based on preliminary experiments and previously published reflectance confocal microscopy criteria of AK and BCC.[20–22] FLSM evaluations were performed in correlation with established criteria of routine histopathology such as nuclear pleomorphism, cellular atypia, tumor nesting, stratum corneum disruption, inflammation, and increased vascularity. Following FLSM evaluation, all lesions were excised for histopathological diagnosis and correlation with routine H&E histology. Fifteen out of 30 were histologically characterized as AK; the remaining 15 were histologically classified as BCC.

2.4.3 *Use of FLSM for noninvasive monitoring of therapy*

We tested the applicability of FLSM for noninvasive monitoring of skin response to therapy in those 15 patients with a diagnosis of BCCs confirmed by routine histopathology. A topical immune response modifier (Imiquimod) was used for

topical treatment for BCC.[23,24] Imiquimod (Aldara, Laboratoires 3 M Santé, Cergy Pontoise Cedex, France) has received Food and Drug Administration approval for the treatment of NMSC and numerous investigations have demonstrated its effectiveness in treating BCC.[23] Local applications of Imiquimod were initiated at the recommended dosing schemes (i.e., three times weekly for six weeks) and patients were evaluated using FLSM at baseline, 3 weeks into therapy, and 8 and 12 weeks after cessation of therapy, respectively. FLSM images were obtained at well-defined evaluation sites and the respective degree of atypia, cellular pleomorphism, and inflammation were noted at different time points. Observational analysis included those FLSM features of BCC established by the initial FLSM evaluation described above. Their presence or absence was recorded in each skin layer and a minimum of four images were captured and stored for repeated analysis at a later time point.

2.5 *Routine Histology*

We obtained 4-mm punch skin biopsies from selected skin sites suspicious for AK or BCC upon clinical evaluation for correlation with FLSM. After fixation with formalin, the 4-μm, paraffin-embedded sections were stained with H&E for histological characterization of the tumor. All cases were examined by a board-certified dermatopathologist. No biopsies were obtained from control sites. Histological evaluation criteria for AK included the presence of parakeratosis (presence of nuclei in the stratum corneum) and hyperkeratosis (increased thickening of the stratum corneum), both of which indicate epidermal hyperproliferation and aberrant epidermal differentiation. Nuclear pleomorphism and cellular atypia appear as variable sizes of keratinocyte nuclei, the eccentric placement of the nuclei, and an aberrant nuclei-to-cytoplasm ratio with atypically enlarged nuclei. The loss of normal epidermal architecture is indicative of aberrant keratinocyte differentiation and notably refers to the loss of the characteristic layering of the epidermis due to the replacement by aberrant, neoplastic keratinocytes. Histological evaluation criteria for BCC include the formation of tumor nests consisting of aberrant basal cells. The polarization of cells gives a monomorphic appearance to the tumor nests, and a characteristic cleft formation may be observed surrounding these tumor lobules. The pleomorphism of the epidermal keratinocytes surrounding BCC nests reflects an aberrant maturation and differentiation of keratinocytes and corresponds to the long-standing actinic damage that has occurred in the affected skin sites. Unspecific criteria of both malignancies include the presence of inflammatory cells, spongiosis (inter- and intracellular edema), and increased vascularity in the superficial dermal layer, all of which reflect an unspecific response to the presence of tumor tissue and neovascularization.

3 Results

3.1 *Fluorescence Confocal Microscopy (FLSM) Findings of Normal Skin*

We have based our analysis on observations previously made by Swindle et al.[13,14] and our findings were in agreement with those obtained in other experiments.[13,18] When imaging the skin in real time starting from the surface and progressing deeper, the most superficial images obtained are from the stratum corneum. The morphological appearance is that of polygonal cells measuring approximately 25 to 40 μm in size, grouped in "islands" separated by skin folds, which appear very dark [Fig. 2(a)]. The stratum granulosum consists of two to four layers of cells, each cell measuring 20 to 25 μm in size. By using FLSM, nuclei can be appreciated as either bright or dark, round to oval structure placed centrally within the cell depending on the distribution of fluorescein as a function of time [Fig. 2(b)]. The cells of the stratum spinosum are arranged in a tight honeycombed pattern of smaller cells, each cell measuring 15 to 20 μm in size, with well-demarcated cell borders.

The deepest layer of epidermis, the basal layer, is seen as dark clusters of cells, each cell measuring about 10 to 12 μm. When imaging at the suprapapillary epidermal plate, the dermoepidermal junction appears as round to oval rings of dark basal cells surrounding dermal papillae, which appear bright due to the homogenous distribution of fluorescein in this layer. A central area of blood flow corresponds to the presence of superficial dermal capillary loops [Fig. 2(c)]. Other features that can be observed in normal skin include hair shafts with pilosebaceous units [Figs. 3(a) and 3(b)]; the latter appear as whorled centrally hollow structures with elliptically elongated cells at the circumference and a central hair shaft. Similarly, eccrine ducts, which appear as bright centrally hollow structures that spiral through epidermis and dermis, can be visualized [Figs. 3(c) and 3(d)].

When looking at the topographical variations of normal skin, patterns vary depending on the site and skin color being evaluated. Chronically sun-exposed skin also demonstrates a thicker and more fissured or wrinkled stratum corneum and more randomly arranged and irregularly shaped dermal papillae. Furthermore, bright reticulated patterns consistent with collagen and irregular elastin fibers may be visualized. According to our preliminary findings, there may be significant numerical variations of epidermal keratinocytes such that the number of keratinocytes is greater in sun-protected sites. The palms and soles are characterized for having an extremely thick stratum corneum and a greater number of eccrine ducts. Similarly, dry skin exhibits more superficial disruptive features in the stratum corneum compared to healthy skin [Figs. 4(a)–4(d)].

3.2 *Fluorescence Confocal Microscopy of Neoplastic Skin Lesions*

3.2.1 *Actinic keratoses (AK)*

FLSM features of AK corresponded well to the established key histopathological features of AK [Fig. 5(a)]. In comparison with normal skin [Fig. 5(b)], FLSM was able to visualize the architectural disarray and keratinocyte pleomorphism at the level of the basal, spinous, and granular layers. [Figs. 5(c) and 5(d)]. Keratinocyte atypia are seen as cells and nuclei, varying in size and orientation. Irregular fluorescein distribution reflects the loss of clear cell-to-cell demarcation. Prominent superficial disruption associated with aberrant differentiation and hyperproliferation of epidermal keratinocytes resulted in detached corneocytes and visualization of bright superficial scale. Exocytosis and mild-to-moderate spongiosis was frequently observed, but the increased vascularity was not consistently visualized using FLSM. The absence of tu-

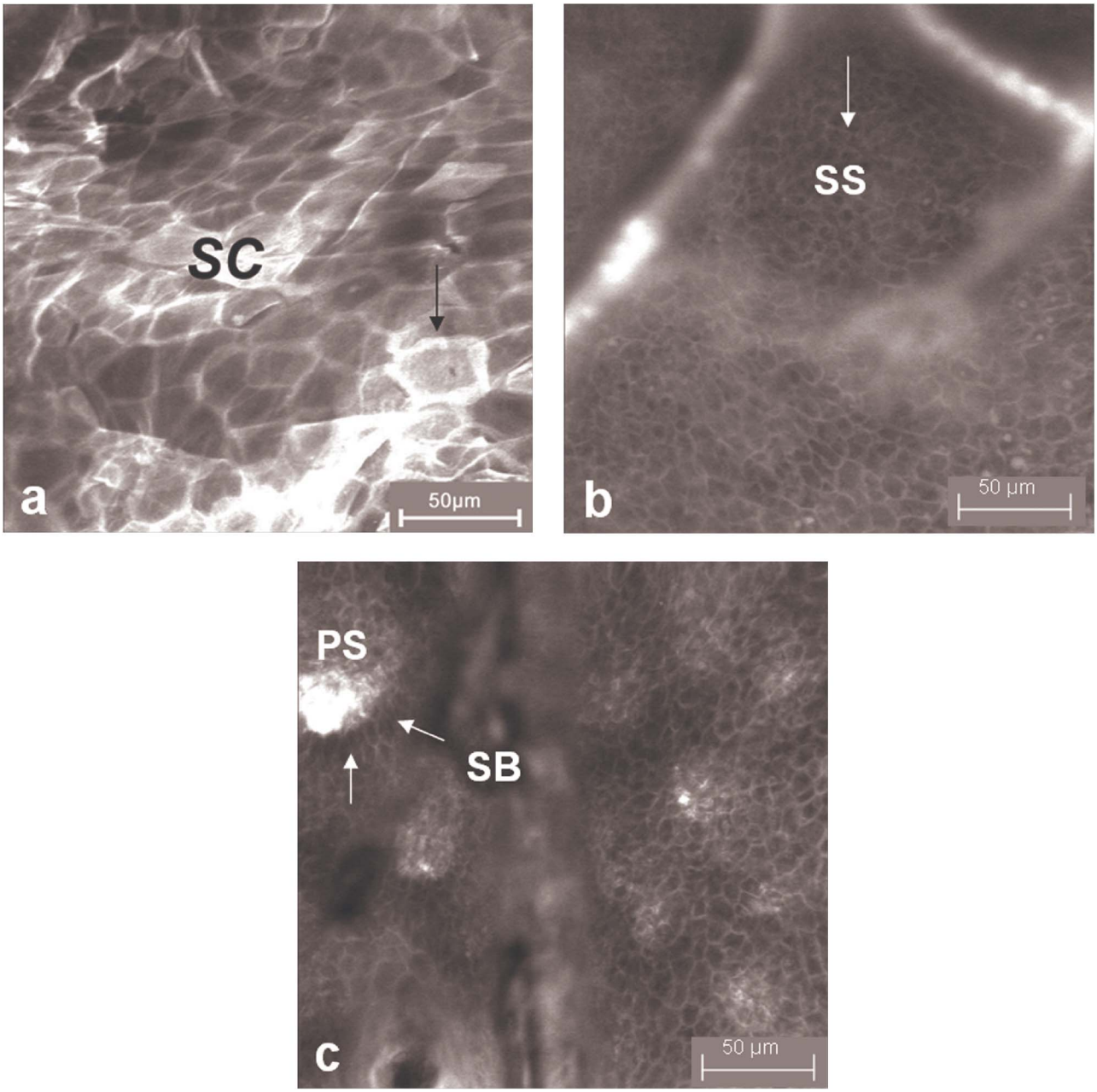

Fig. 2 Illustration of the horizontal FLSM morphology of normal skin. (a) FLSM morphology of stratum corneum (SC) shown. Corneocytes appear as bright structures of polygonal shape, 25 to 40 μm in diameter. Due to the anucleated nature of corneocytes, no significant uptake of fluorescein is observed, leaving the surrounding intercellular spaces to appear as a bright rim due to accumulated fluorescein (black arrow). (b) Representative image of the stratum spinosum (SS) as obtained by FLSM. Spinous keratinocytes are seen at 25 to 50 μm below the stratum corneum. The dark oval structures correspond to the spinous keratinocytes (SS), and intercellular spaces appear bright. Rhomboidal image artifact corresponds to accumulation of fluorescein in overlying skin folds. (c) Basal keratinocytes in the stratum basale (SB), surrounding each papillary structure (PS); basal keratinocytes appear darker than surrounding keratinocytes (white arrows). The center of each papilla appears bright due to the abundance of collagen (PS). All images were obtained approximately 10 to 15 min after injection of fluorescein. All images resolved in gray scale; respective FOV=250×250 μm (scale bar, 50 μm).

mor nesting served as a distinguishing feature against BCC.

3.2.2 *Basal cell carcinoma* (*BCC*)

FLSM was able to detect the morphologic characteristics of BCC that were in correlation with routine histology. Tumor nests corresponded to the presence of islands of atypical basal cells that are monomorphic in shape [Fig. 6(c)]. Large, elongated nuclei were often oriented along the same axis, resulting in an overall polarized appearance. Areas of clefting demarcated the tumor nests against surrounding epidermal structures [Fig. 6(d)]. A superficial inflammatory infiltrate was visualized as multiple, round to oval structures of 8 to 10 μm in diameter [Fig. 6(d)]. Prominent atypia and pleomorphism of epidermal keratinocytes compared well to that observed in

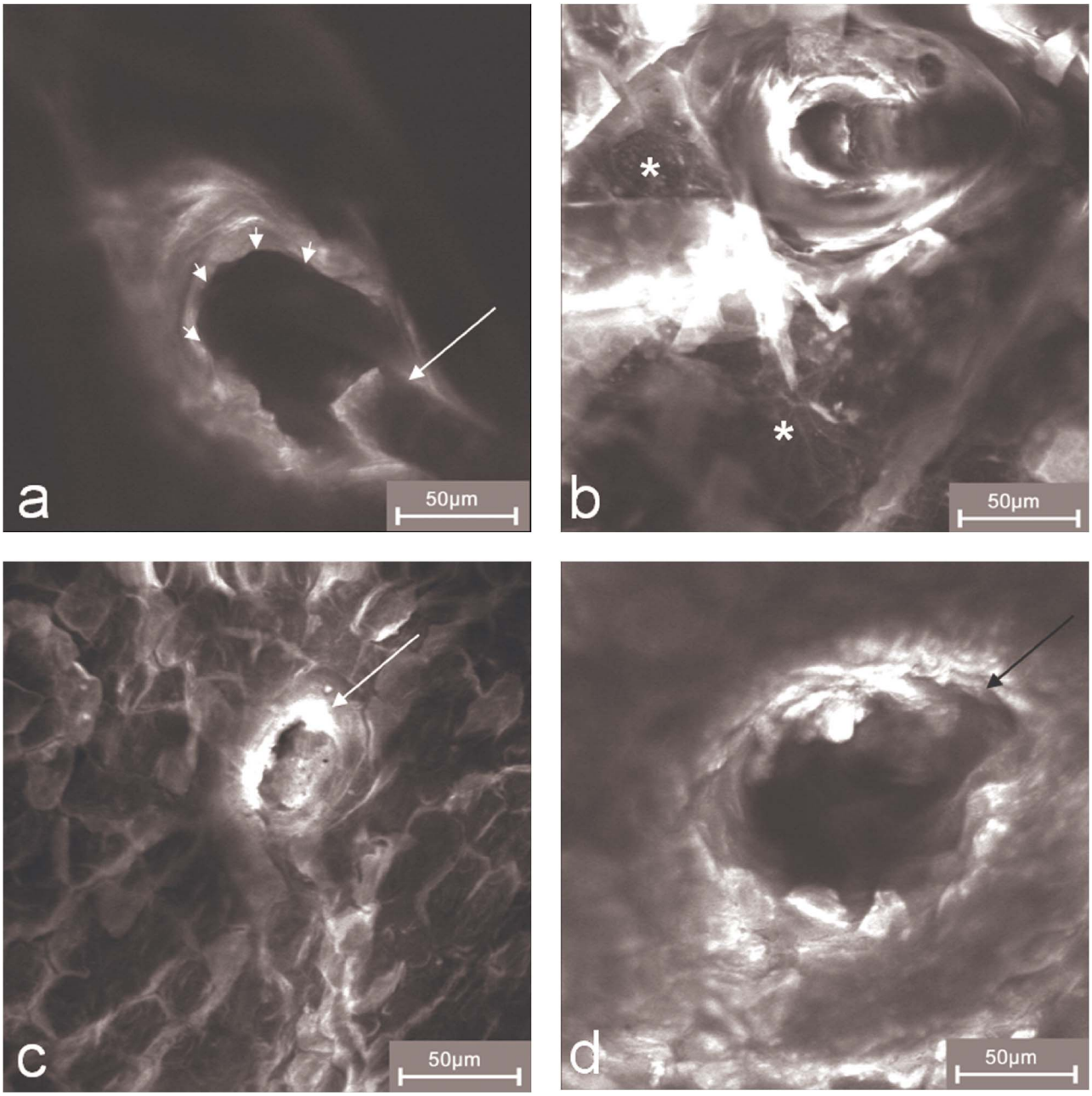

Fig. 3 FLSM morphology of adnexal structures in normal skin. Panels (a) and (b) correspond to hairshafts with associated pilosebaceous structures. The white arrow indicates hair appearing as a dark longitudinal structure within the anatomic outline of hairshaft, which appears as a dark, hollow, canalicular structure (white arrowheads). (b) Asterisks ($*$) correspond to areas of associated sebaceous glands. Panels (c) and (d) represent FLSM images of eccrine ducts imaged on the palm. Panel (c) shows the most superficial aspect of the eccrine duct with the narrow palmar opening indicated by a white arrow. Panel (d) corresponds to the FLSM image of an eccrine gland obtained from palmar skin; black arrow indicates the wide lumen of the eccrine gland, lined circumferentially by eccrine epithelial cells. All images resolved in gray scale; respective FOV = 250 × 250 μm (scale bar, 50 μm).

AK. At the level of the dermoepidermal junction [Fig. 7(a)], the aberrant epidermal cells interfere with the normal honeycomb pattern of normal skin [Fig. 7(b)] and result in the disruption of dermal papillary architecture [Fig. 7(c)]. Dermal papillae exhibit abundant blood vessels with prominent tortuosity as well as increased blood vessel dilatation [Fig. 7(d)–7(f)].

3.3 *FLSM for Monitoring of Therapy*

Upon initial FLSM examination, BCC sites showed characteristic atypia of basal keratinocytes with loss of cell-to-cell demarcation, tumor nesting, and nuclear pleomorphism [Fig. 8(a)]. Similar evaluations following localized Imiquimod application showed spongiosis and an inflammatory infiltrate

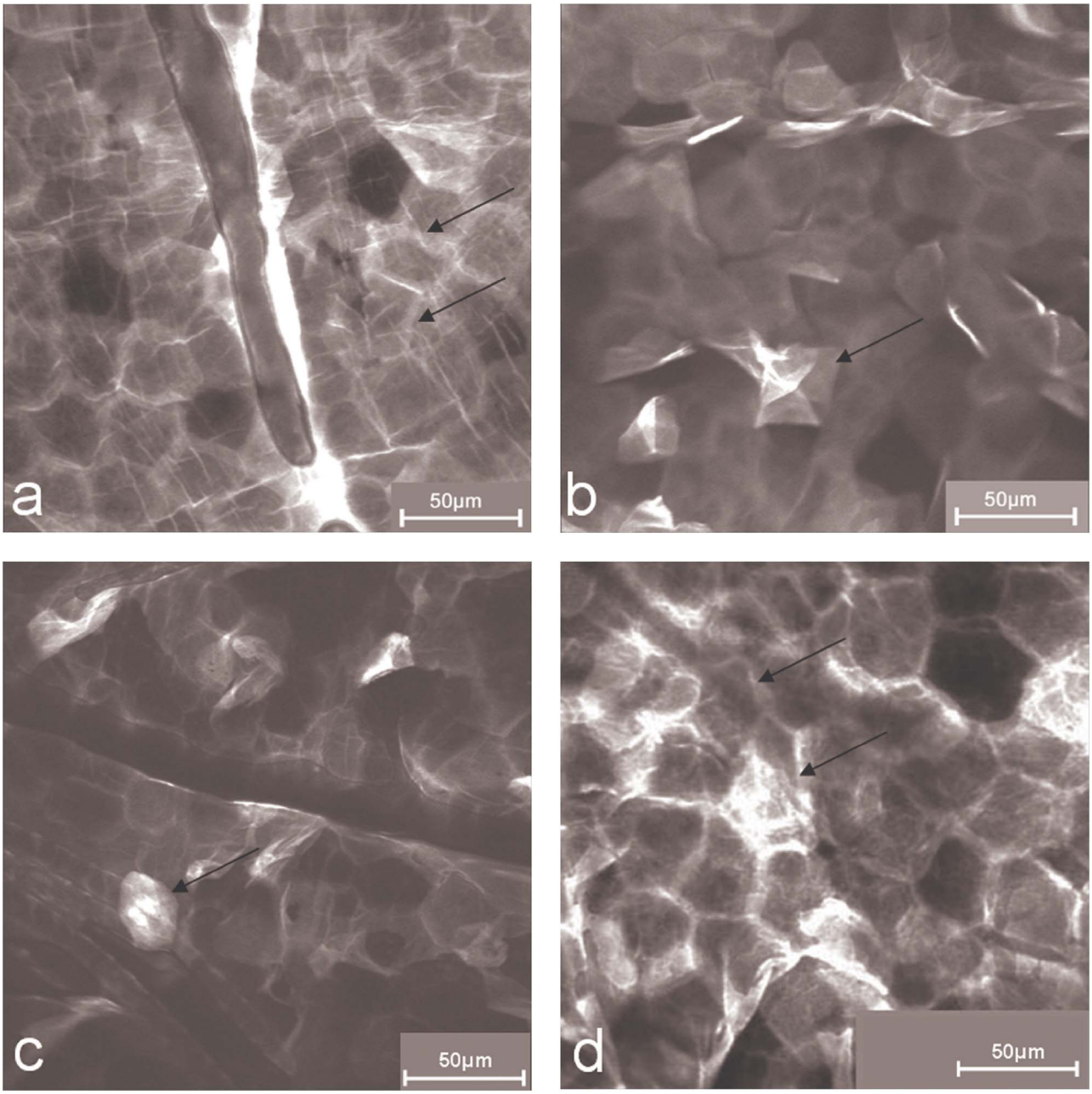

Fig. 4 FLSM images of different physiologic and pathophysiologic states of the stratum corneum (SC). Panels (a) and (b) show corresponding images of SC in normal skin (a) and dry skin (b), respectively. Black arrows denote individual detached corneocytes. Normal skin (a) exhibits a homogenous, cohesive pattern of polygonal cells with regular openings of the eccrine ducts. Intercellular brightness relates to intercellular or cytoplasmatic fluorescein accumulation. No detached cells can be appreciated. Dry skin (b) shows decreased cohesiveness of the SC with individual detached corneocytes and partial widening of the eccrine openings. Similarly, (c) and (d) show the SC of a study participant with dry skin before (c) and after (d) the application of moisturizer. The black arrow in (c) indicates the presence of detached corneocytes as a sign of superficial SC disruption. After the application of moisturizer, (d), increased homogeneity and cohesiveness of the SC layer were noted (black arrows). All images resolved in gray scale; respective FOV=250×250 μm (scale bar, 50 μm).

seen as multiple, round to oval structures with bright appearance. At three weeks into treatment, FLSM illustrated an inhomogenous appearance of pleomorphic basal cells and atypical keratinocytes remained. Residual atypia, nuclear pleomorphism, and a scarce inflammatory infiltrate can be observed. [Fig. 8(b)]. At 8 and 12 weeks after initiation of therapy, a normalization of epidermal architecture can be observed by FLSM in selected treatment sites, and residual atypia and nuclear pleomorphism was still detectable in others [Fig. 8(c)].

4 Discussion

There are several advantages of *in vivo* laser scanning microscopy (LSM) over conventional histology. The imaging is painless and noninvasive, causing no tissue damage or alter-

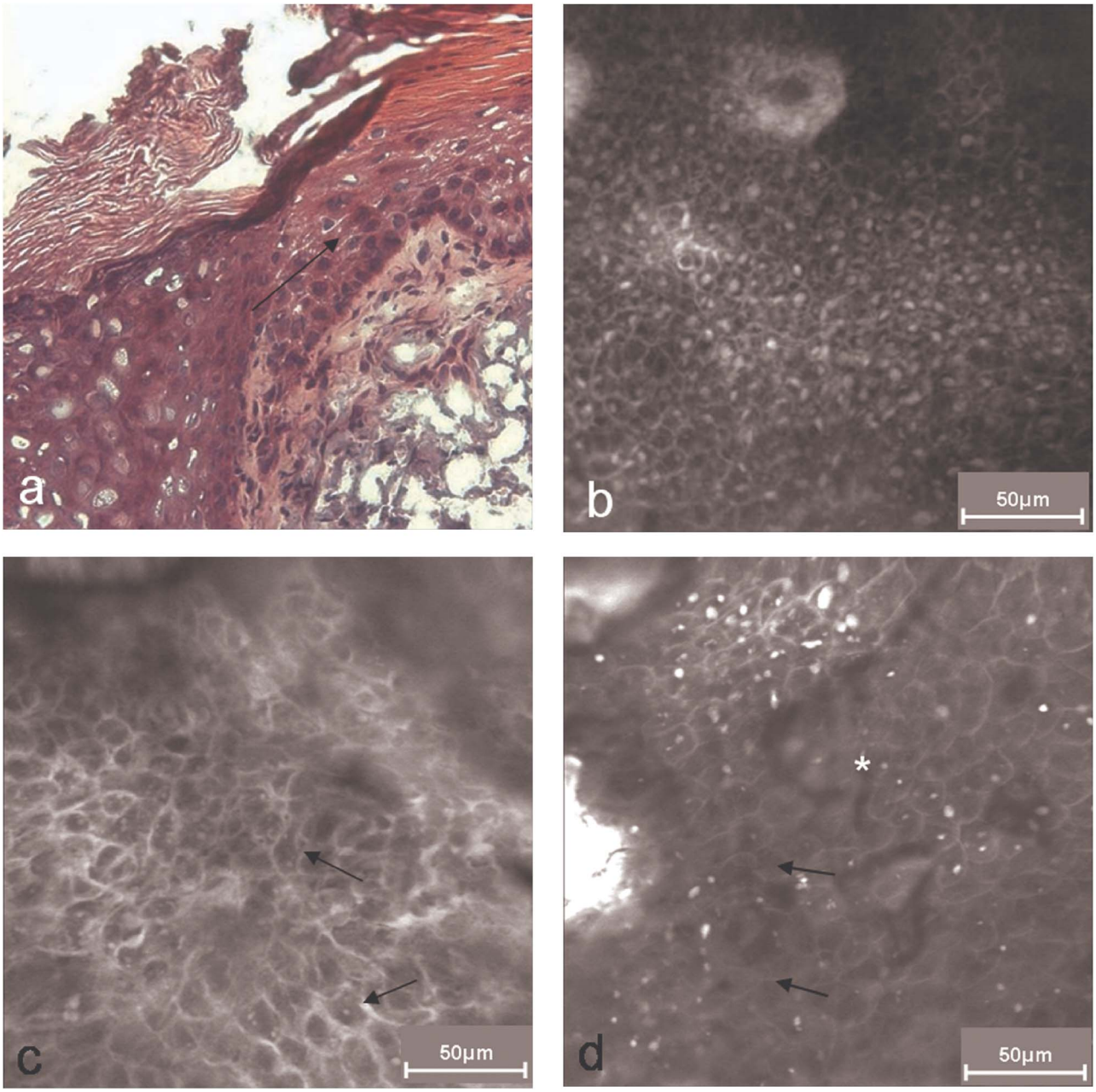

Fig. 5 FLSM morphology of AK in correlation with routine H&E and in comparison with normal skin. Panel (a) shows vertical H&E section (400× original magnification) of AK with noted epidermal pleomorphism, parakeratosis, hyperkeratosis, and architectural disarray (black arrow indicating atypical keratinocyte). Panel (b) corresponds to *en face* FLSM image of normal skin showing spinous keratinocytes with homogenous appearance. Nuclei appear as uniform, bright, centrally placed structures within dark cytoplasm. Intercellular spaces appear as surrounding bright structures, indicating clear cell-to-cell demarcation. Panel (c) corresponds to *en face* FLSM image of AK. Image obtained at the level of the granular layer; keratinocytes showing enlarged, pleomorphic nuclei with haphazard orientation (black arrows) and noted loss of cell-to-cell demarcation. Atypical nuclei vary in size and are often placed eccentrically within dark cytoplasm. Panel (d) corresponds to *en face* FLSM image of AK obtained at the level of the spinous layer. Inhomogeneous staining of nuclei and irregular cell-to-cell demarcation (*) illustrate the pleomorphism of atypical spinous keratinocytes (black arrows). All images resolved in gray scale; respective FOV = 250 × 250 μm (scale bar, 50 μm).

ation by processing or staining. Another aspect is the rapidity with which the data can be collected, and the ability of LSM for repeated evaluations of dynamic processes in real time.[14,18–22] These may include the longitudinal evaluation of physiologic events, disease evolution over time, or response to therapy.[24,25] In that regard, FLSM characterization of neoplastic lesions is an important area for research, with the potential to aid in the noninvasive diagnosis and management. With the advent of newer less invasive or topical therapies, it appears desirable to employ noninvasive diagnostic tools for evaluation of tumor subtypes, tumor margins, and treatment responses.[14,26]

In the present study, FLSM was used for diagnosis and therapeutic monitoring of NMSC in reference to normal skin

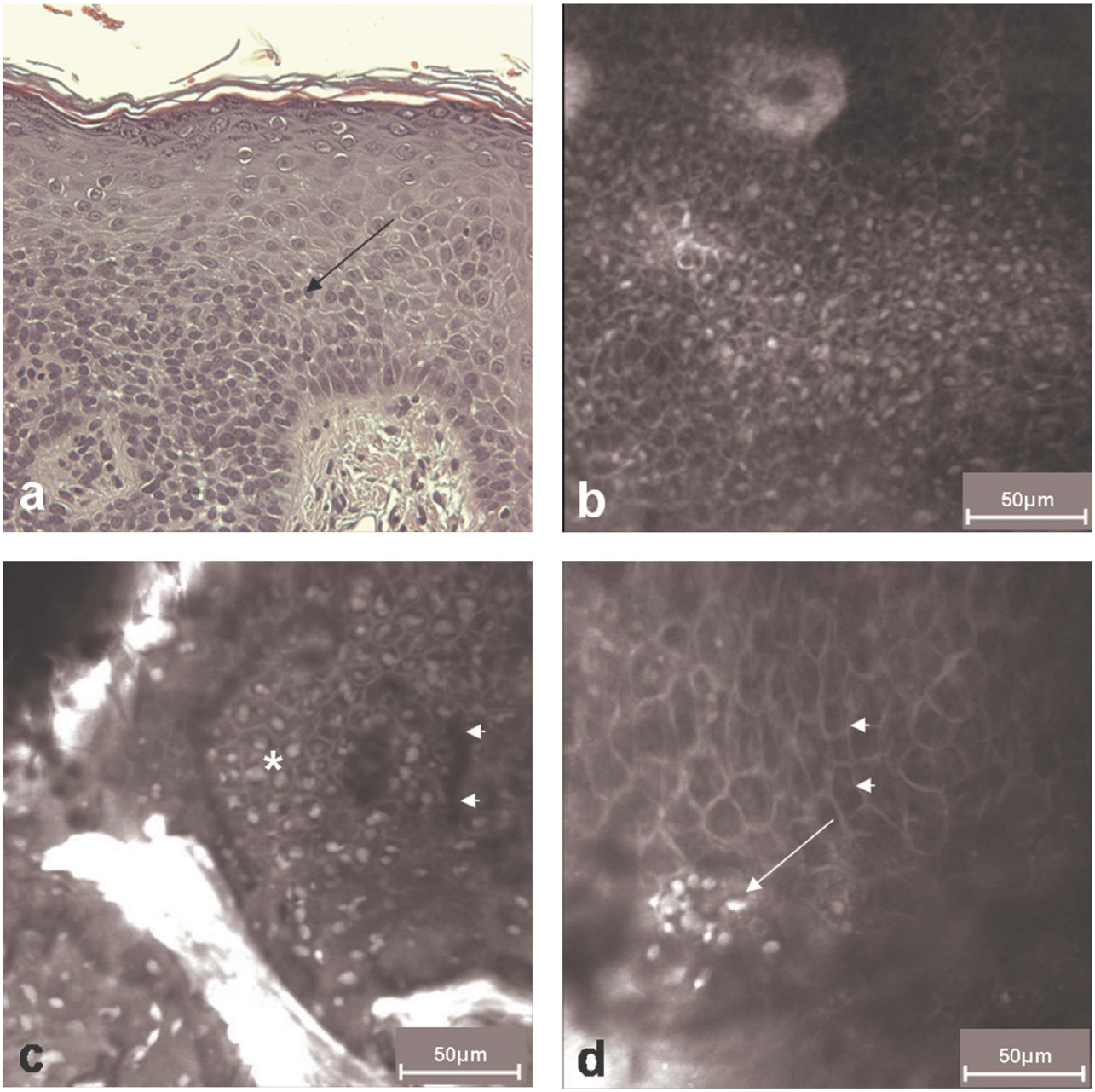

Fig. 6 Correlation between vertical H&E and FLSM morphology of BCC, superficial type. Panel (a) corresponds to vertical H&E showing nuclear polarization and epidermal pleomorphism. Arrow denoting atypical keratinocytes and aberrant proliferation of basal cells. Individual nuclei appear dark on H&E stains. Panel (b) corresponds to representative *en face* FLSM morphology of normal skin. Individual nuclei appear as bright, centrally placed structures within the dark appearing cytoplasm; each spinous keratinocyte is surrounded by a bright rim due to intercellular and cytoplasmatic accumulation of fluorescein, and cells appear morphologically homogenous. Panel (c) corresponds to *en face* FLSM morphology of BCC, atypically large cells with noted heterogeneity of fluorescein uptake and aberrant cell morphology (white arrowheads). The presence of inflammatory cells is shown as a cluster of small, round to oval, bright cells of 8 to 10 μm in diameter (white arrow). Image obtained at the level of the granular layer. Panel (d) illustrates *en face* FLSM morphology of lobular tumor nests (white *). Lateral tumor edges (white arrowheads) appear surrounded by dark areas of clefting (white arrows), demarcating tumor nests; images were obtained at the level of the spinous layer. All images resolved in gray scale; respective FOV = 250 × 250 μm (scale bar, 50 μm).

and correlation with routine histology. Several characteristic differences in the skin morphology, well known from histology, could be detected by FLSM and allowed the distinction of diagnostic features of AK and BCC. When evaluating AK, the most characteristic feature was the disruption of the stratum corneum and epidermal pleomorphism, which—in the *absence* of tumor nesting—was more indicative of AK. It should be mentioned, however, that an accurate assessment of the dermoepidermal junction may be difficult in the presence of significant hyperkeratosis. Interestingly, corresponding FLSM findings of AK were also present in areas where no pathologic findings were noted upon initial clinical examina-

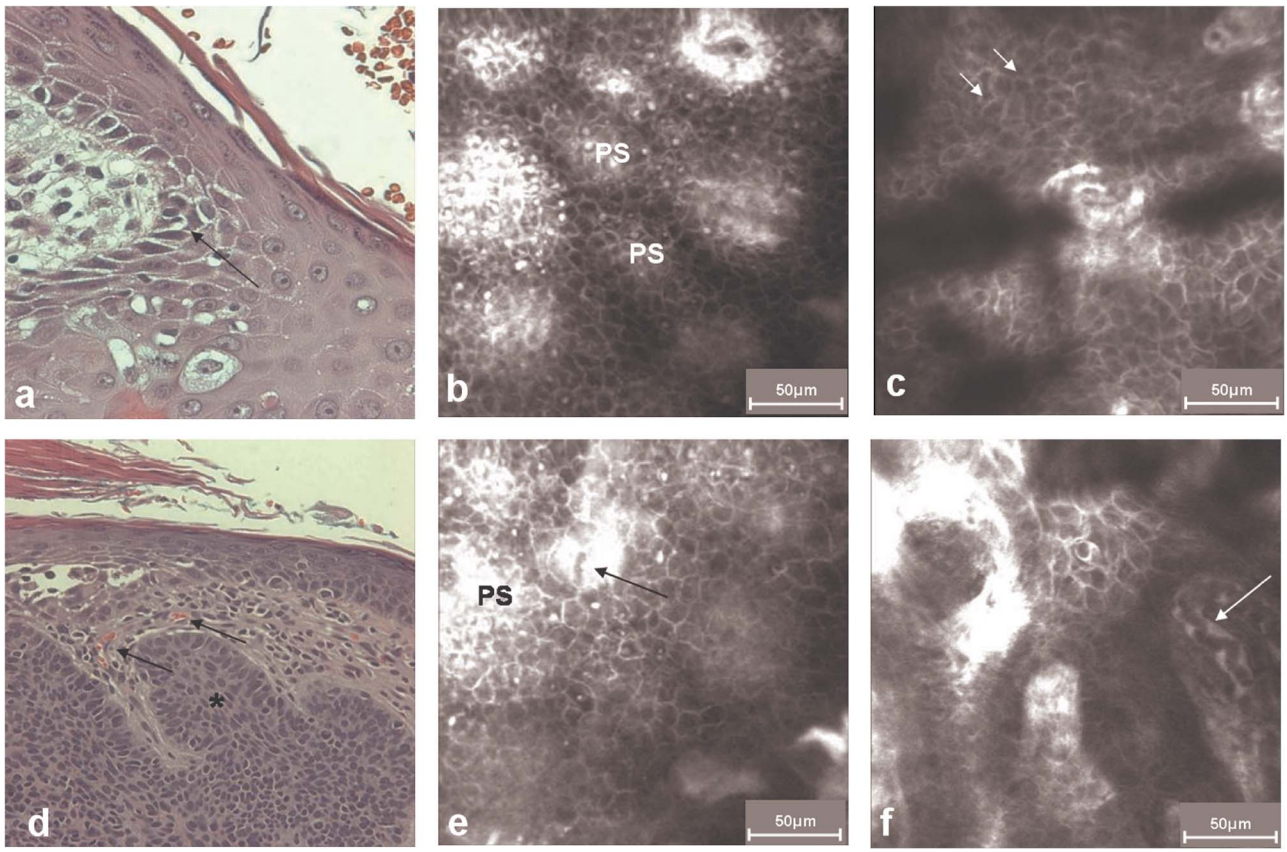

Fig. 7 FLSM morphology of BCC in correlation with routine H&E and in comparison with normal skin. Panel (a) represents a *vertical* H&E section of BCC illustrating the aberrant morphology of basal cells at the level of the dermoepidermal junction with widening of the intercellular spaces (arrow). Panel (b) corresponds to representative FLSM morphology of normal skin with homogenous appearance of spinous keratinocytes; selected papillary structures indicated by (PS). Panel (c) corresponds to FLSM morphology of BCC, showing architectural disruption of the epidermis with pleomorphism of basal keratinocytes, decreased cell-to-cell demarcation, and widening of the intercellular spaces (white arrows); no regular papillary structures can be identified. Panels (d) to (f) illustrate the aberrant morphology of tumor vasculature. Panel (d) corresponds to vertical H&E histology (40×) of BCC with nesting of atypical basal cells in the upper dermis (black *) and dilated blood vessels in the superficial dermis (black arrows). Panel (e) corresponds to FLSM of normal skin at the level of the dermoepidermal interface with small vessel diameter (black arrowhead). Blood vessels are shown as dark canalicular structures within the tip of the characteristic bright appearance of dermal papillae. Panel (f) corresponds to FLSM of BCC at the level of the dermoepidermal interface; The white arrow denotes the increased vessel diameter and elongated appearance of atypical vasculature. All images resolved in gray scale; respective FOV=250×250 μm (scale bar, 50 μm).

tion, indicating the ability of FLSM to detect subclinical keratinocyte atypia. On the other hand, BCC showed comparable epidermal pleomorphism and the characteristic nesting of atypical basal cells was easily visualized using FLSM. BCC did not commonly present with hyperkeratosis, but demonstrated increased blood vessel tortuosity.

To allow the noninvasive monitoring of treatment response to Imiquimod, all corresponding FLSM features for superficial BCC were evaluated at baseline and variable time points during and after therapy. Our preliminary observations showed an initial increase of inflammatory cells relating to local immune response, and these findings subsided with cessation of therapy. The vascular dilatation or increased vascularization of treatment sites was observed after a course of 6 weeks of topical treatment and persisted at the 12 week followup, relating to the induction of neovascularization following Imiquimod therapy as described in previous reports.[23,24,27]

Previous studies have used RCM in the monitoring of therapeutic response,[24–26] however, no studies using FLSM have been published to date. Although RCM allows the distinction of AK and BCC based entirely on endogenous contrast and tissue reflectivity,[15] FLSM allowed the visualization of structures through intra- and intercellular accumulation of exogenously applied fluorophores. Nuclear morphology is readily identified in both systems, yet when compared to RCM, where reflectance noise is a potential confounding factor in the evaluation, FLSM allows the visualization of cellular and nuclear dimensions based on fluorescein distribution over time.[13,14] Cell-to-cell demarcation in normal skin is clearly distinguishable using FLSM due to the accumulation of fluorescein in the intercellular compartment. In contrast, barrier dysfunction of diseased skin may be associated with increased permeability of cellular membranes such that cell-to-cell demarcations can be less defined. With FLSM timing of the evaluation remains an important aspect of the evalua-

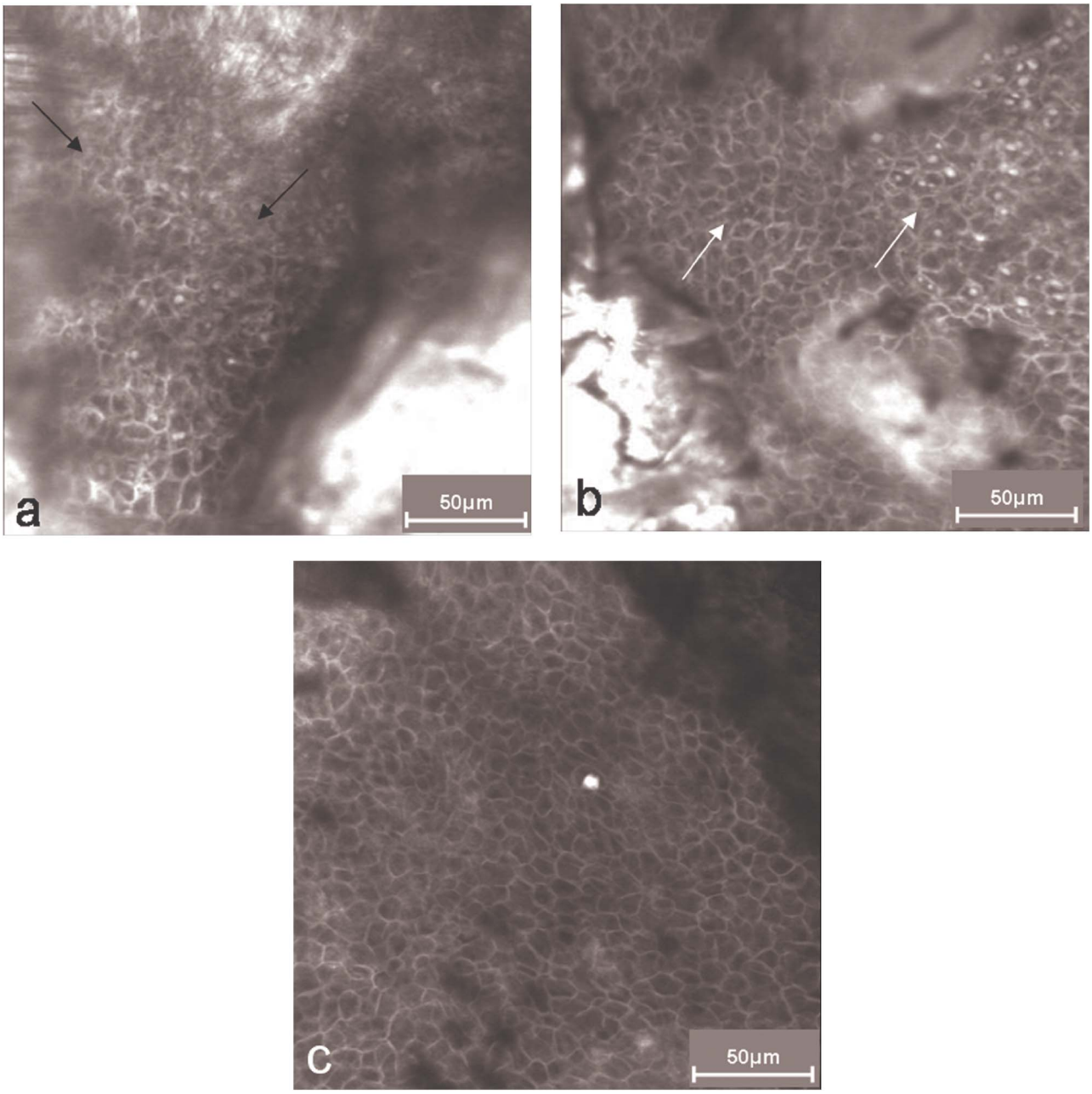

Fig. 8 Example of FLSM for noninvasive monitoring of treatment response in BCC. Panel (a) corresponds to FLSM image of superficial BCC obtained at the level of the spinous layer prior to treatment with Imiquimod. Increased brightness is associated with architectural disruption, loss of clear cell-to-cell demarcation, and irregular staining of nuclei; fluorescein accumulation indicates nuclear atypia and cellular polymorphism (black arrows). Brightness in lower-right corner relates to the image artifact. Panel (b) corresponds to FLSM image obtained three weeks after the start of treatment. Inhomogeneous appearance of pleomorphic spinous keratinocytes (white arrows) remains. Panel (c) was imaged eight weeks posttreatment. The characteristic honeycombed pattern of the epidermis corresponds to increased normalization of epidermal architecture and homogeneous staining relates to improved cell-to-cell demarcation. Images resolved in gray scale; FOV=250×250 μm. (scale bar, 50 μm).

tion, because the distribution of fluorescein follows a characteristic dynamic in live skin. RCM, on the other hand, allows an evaluation *without* exogenous contrast agents, thus underlining the noninvasive nature of this technology.[15] The reproducibility of features appears comparable in both systems, with a systematic evaluation yet to be conducted. Overall, the ability of FLSM to image skin noninvasively and in real time without any discomfort makes it a promising tool in clinical dermatology.

Although there are many benefits of FLSM, there are also some limitations. The current technology is complex and expensive and thus not widely available to researchers and clinicians. Another potential limitation may be that imaging requires the application of exogenous fluorophores and the intraepidermal injection of fluorescein. With respect to image interpretation, the differences are often subtle and difficult to appreciate, such that a reliable interpretation is often based on

correlation with normal skin or in reference with routine histology.

5 Summary

FLSM offers numerous potential applications for the advancement of medical research and clinical care by evaluating the status of normal skin, dynamic skin processes such as secretory and eccrine functions, and/or the management of skin disease. Our findings indicate that FLSM may be a feasible tool to monitor therapeutic skin response, thereby evaluating the effectiveness of topical therapies for NMSC noninvasively and *in vivo*. FLSM may allow a systematic, noninvasive histomorphometric evaluation of AK and BCC, potentially aiding in the detection of subclinical AK and early therapeutic management. The findings presented herein are of observational and preliminary nature, and further studies are warranted to corroborate our findings.

Acknowledgments

The authors would like to acknowledge OptiScan Ltd., Australia for providing the Stratum microscope for the study and for their help with the preparation of this manuscript. We would like to thank the Foundation "Skin Physiology" of the Donor Association for German Science and Humanities for their financial support.

References

1. C. J. Cockerell, "Histopathology of incipient intraepidermal squamous cell carcinoma ('actinic keratosis')," *J. Am. Acad. Dermatol.* **42**, 11–17 (2000).
2. S. T. Guenther, R. M. O. Hurwitz, L. J. U. Buckel, and H. R. Gray, "Cutaneous squamous cell carcinomas consistently show histologic evidence of in situ changes: A clinicopathologic correlation," *J. Am. Acad. Dermatol.* **41**, 443–448 (1999).
3. R. Marks, G. Rennie, and T. S. Selwood, "Malignant transformation of solar keratoses to squamous cell carcinoma," *Lancet* **1**, 795–797 (1988).
4. E. Diamandidou, P. R. Cohen, and R. Kurzrock, "Mycosis fungoides and Sezary syndrome," *Blood* **88**, 2385–2409 (1996).
5. M. Vogt, B. Paul, S. Scharenberg, R. Scharenberg, and H. Ermert, "Development of a high frequency ultrasound skin imaging system: Optzimization utilizing time domain reflectometry and network analysis," *Proc.-IEEE Ultrason. Symp.* pp. 2137–2140 (2004).
6. M. Vogt, K. Kaspar, P. Altmeyer, K. Hoffman, and S. El Gammal, "High frequeny ultrasound for high resolution skin imaging," *Frequenz* **55**, 12–20 (2001).
7. F. Mirrashed and J. C. Sharp, "*In vivo* morphological characterization of skin by MRI microimaging methods," *Skin Res. Technol.* **10**, 14–22 (2004).
8. P. J. Caspers, G. W. Lucassen, E. A. Carter, H. A. Bruining, and G. J. Puppels, "*In vivo* confocal Raman microspectroscopy of the skin: Noninvasive determination of molecular concentration profiles," *J. Invest. Dermatol.* **116**, 434–442 (2001).
9. M. C. Pierce Strasswimmer, J. Hyle Park B, J. F. Cense, and B. deBoer, "Advances in optical coherence tomography imaging for dermatology," *J. Invest. Dermatol.* **123**, 458–463 (2004).
10. A. Yaroslavsky, V. Neel, and R. R. Anderson, "Fluorescence polarization imaging for delineating nonmelanoma skin cancers," *Opt. Lett.* **1**(29), 2010–2012 (2004).
11. K. Konig, P. T. So, W. W. Mantulin, B. J. Tromberg, and E. Gratton, "Two-photon excited lifetime imaging of autofluorescence in cells during UVA and NIR photostress," *J. Microsc.* **183**, 197–204 (1996).
12. A. Boyde, S. J. Jones, M. L. Taylor, L. A. Wolfe, and T. F. Watson, "Fluorescence in the tandem scanning microscope," *J. Microsc.* **157**, 39–49 (1990).
13. L. D. Swindle, S. G. Thomas, M. Freeman, and P. M. Delaney, "View of normal human skin *in vivo* as observed using fluorescent fiber-optic confocal microscopic imaging," *J. Invest. Dermatol.* **121**, 706–712 (2003).
14. L. Swindle, M. Freeman, B. Jones, and S. Thomas, "Fluorescence confocal microscopy of normal human skin and skin lesions *in vivo*," *Skin Res. Technol.* **9**(2), 167 (2003).
15. M. Rajadhyaksha and S. Gonzalez, "Real-time *in vivo* confocal fluorescence microscopy," in *Handbook of Biological Fluorescence*, M.-A. Mycek and B. W. Pogue, Eds. Marcel Dekker, New York (2003).
16. J. Lademann, H. Richter, N. Otberg, F. Lawrenz, U. Blume-Peytavi, and W. Sterry, "Application of a dermatological laser scanning microscope for investigation in skin physiology," *Laser Phys.* **13**(5), 1–5 (2003).
17. M. Minsky, "Microscopy apparatus," U.S. Patent No. 3013467, 1957 (1961).
18. M. Huzaira, F. Rius, M. Rajadhyaksha, R. R. Anderson, and S. González, "Topographic variations in normal skin histology, as viewed by *in vivo* reflectance confocal microscopy," *J. Invest. Dermatol.* **116**(6), 846–852 (2001).
19. S. González, M. Rajadhyaksha, and R. R. Anderson, "Confocal imaging of proliferative cutaneous lesion margen *in vivo*," *J. Invest. Dermatol.* **111**(3), 538–539 (1998).
20. D. Agasshi, R. R. Anderson, and S. González, "Confocal laser microscopic imaging of actinic keratoses *in vivo*: A preliminary report," *J. Am. Acad. Dermatol.* **43**, 42–48 (2000).
21. S. González and Z. Tannous, "Real-time *in vivo* confocal reflectance microscopy of basal cell carcinoma," *J. Am. Acad. Dermatol.* **47**, 869–874 (2002).
22. S. Nori, F. Rius-Diaz, J. Cuevas, M. Goldgeier, P. Jaen, A. Torres, and S. González, "Sensitivity and specificity of reflectance mode confocal microscopy for *in vivo* diagnosis of basal cell carcinoma: A multicenter study," *J. Am. Acad. Dermatol.* **51**, 923–930 (2004).
23. C. A. Burns and M. D. Brown, "Imiquimod for the treatment of skin cancer," *Dermatol. Clin.* **23**(1), 151–164 (2005).
24. A. Torres, A. Niemeyer, B. Berkes, A. Marra, C. Schanbacher, S. González, M. Owens, and B. Morgan, "5% Imiquimod cream and reflectance-mode confocal microscopy as adjunct modalities to Mohs' micrographic surgery for treatment of basal cell carcinoma," *Dermatol. Surg.* **30**, 1462–1469 (2004).
25. D. Marra, A. Torres, C. F. Schanbacher, and S. González, "Detection of residual basal cell carcinoma by *in vivo* confocal microscopy. Detection of residual basal cell carcinoma by *in vivo* confocal microscopy," *Dermatol. Surg.* **31**(5), 538–541 (2005).
26. M. Goldgeier, C. A. Fox, J. M. Zavislan, D. Harris, and S. González, "Noninvasive imaging, treatment, and microscopic confirmation of clearance of basal cell carcinoma," *Dermatol. Surg.* **29**, 205–210 (2003).
27. R. F. Martin-Garcia, "New insights into imiquimod's mechanisms of action," *J. Drugs Dermatol.* **3**(3), 247–249 (2004).
28. C. Suihko, L. D. Swindle, S. G. Thomas, and J. Serup, "Fluorescence fibre-optic confocal microscopy of skin *in vivo*: Microscope and fluorophores," *Skin Res. Technol.* **11**, 254–267 (2005).